

Dalton Transactions

An international journal of inorganic chemistry

Accepted Manuscript

This article can be cited before page numbers have been issued, to do this please use: M. Shao, X. Liu, Y. Sun, S. Dou, Q. Chen, X. Yuan, L. Tian and Z. Liu, *Dalton Trans.*, 2020, DOI: 10.1039/D0DT02408B.



This is an Accepted Manuscript, which has been through the Royal Society of Chemistry peer review process and has been accepted for publication.

Accepted Manuscripts are published online shortly after acceptance, before technical editing, formatting and proof reading. Using this free service, authors can make their results available to the community, in citable form, before we publish the edited article. We will replace this Accepted Manuscript with the edited and formatted Advance Article as soon as it is available.

You can find more information about Accepted Manuscripts in the [Information for Authors](#).

Please note that technical editing may introduce minor changes to the text and/or graphics, which may alter content. The journal's standard [Terms & Conditions](#) and the [Ethical guidelines](#) still apply. In no event shall the Royal Society of Chemistry be held responsible for any errors or omissions in this Accepted Manuscript or any consequences arising from the use of any information it contains.

SCHOLARONE™
Manuscripts

Preparation and anticancer mechanism of configuration-controlled Fe(II)-Ir(III) heteronuclear metal complexes

Mingxiao Shao, Xicheng Liu*, Yiwei Sun, Shuaihua Dou, Qi Chen, Xiang-Ai Yuan, Laijin Tian, Zhe Liu*

Institute of Anticancer Agents Development and Theranostic Application, The Key Laboratory of Life-Organic Analysis and Key Laboratory of Pharmaceutical Intermediates and Analysis of Natural Medicine, School of Chemistry and Chemical Engineering, Qufu Normal University, Qufu 273165, China.

*Corresponding author, (X. Liu) *E-mail:* chemlxc@163.com; Fax: 0086-537-4456301; (Z. Liu) *E-mail:* liuzheqd@163.com, Fax: 0086-537-4456301.

Abstract

Series of configuration-controlled Fe(II)-Ir(III) heteronuclear metal complexes, including ferrocene and half-sandwich iridium(III) complex units, have been designed and prepared. These complexes show better anticancer activity than cisplatin under the same conditions, especially for *cis*-configurational one. Laser confocal verifies complexes follow a non-energy-dependent cellular uptake mechanism, accumulate in lysosomes (Pearson co-localization coefficient: ~ 0.7), lead to lysosomal damage, and eventually induce apoptosis. These complexes can decrease the mitochondrial membrane potential, disturb the cell cycle, catalyze the oxidation of nicotinamide-adenine dinucleotide (NADH) and increase the levels of intracellular reactive oxygen species (ROS), follow an anticancer mechanism of oxidation. Additionally, complexes could bind to serum protein, and transport through it. Above all, Fe(II)-Ir(III) heteronuclear metal complexes hold promise as potential anticancer agents for further study.

Keywords: Ferrocene; Iridium(III) complex; Lysosome-targeted; Anticancer

1 Introduction

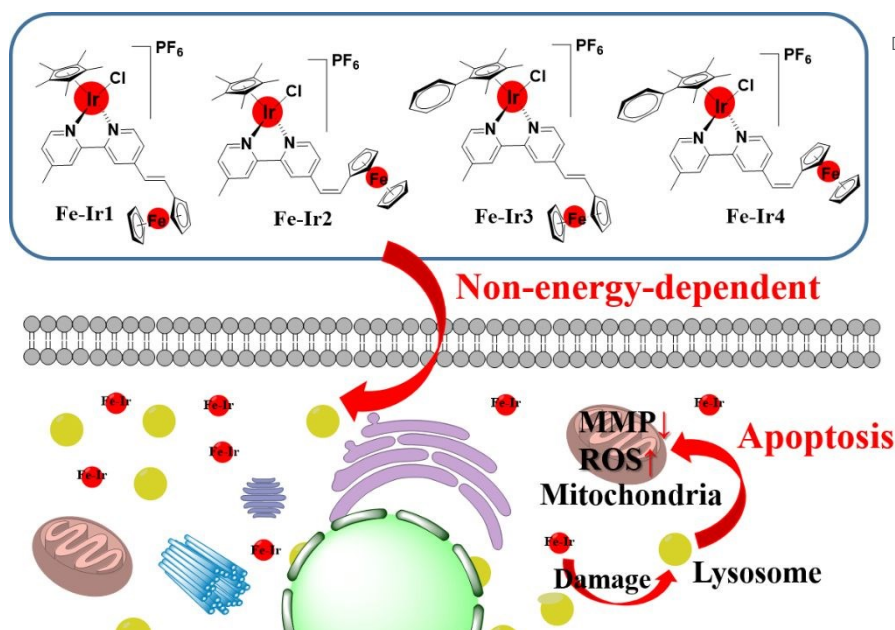
Recently, organometallic compounds, which have at least one metal-carbon bond, have aroused wide concern due to their unique chemical structure and favourable biological activities [1]. Among them, ferrocene and iridium(III) complexes, which have a sandwich structure ($\eta^5\text{-(C}_5\text{H}_5)_2\text{Fe}$) and half-sandwich structure ($[(\eta^5\text{-Cp}^*)\text{Ir(L}^{\wedge}\text{L)Cl}]\text{PF}_6$), have shown extensive applications in various fields, including bio-organometallic chemistry, polymer chemistry, organic synthesis, materials science, crystal engineering and electrochemistry, especially in the anticancer drug design and development [2-4].

Cancer is the second leading cause of death in developed nations according to health organizations. It has been estimated that approximately 1,806,590 cancer cases will be diagnosed in the United States in 2020, which is equivalent to approximately 4,950 new cases each day of the year [5]. Although various organic small molecules and biological derivatives have been widely used for anticancer treatment, platinum-based metallodrugs have attracted attention because of their unique biological and chemical properties [6-8]. Ferrocene and its derivatives, typical organometallic complexes with advantages such as reversible redox properties, low toxicity, low cost and inherent stability in air, are currently being evaluated as anticancer agents [9-12]. Studies have shown that the oxidation state of the ferrocene moiety plays a crucial role in its cytotoxic actions and is involved in inducing the accumulation of reactive oxygen species ($^1\text{O}_2$)

via an oxidation-related mechanism [13-15]. Additionally, some derivatives of ferrocene have been used as ligands to form many types of heteronuclear metal complexes, which have exhibited an important influence on the coordination behaviour of these ligands, and further affect their biological activity *in vitro* [16]. In general, the anticancer potential of ferrocene is lower than that of other metallodrugs but can be improved by combining it with other transition metal complexes [17]. Ferrocenylpyridines, ferrocenylphenylpyridines and 1,1'-di(2-pyridyl)ferrocene ligands and their platinum, palladium, rhodium, and iridium complexes were screened for activity against two human cancer cell lines [18]. At least two of the complexes displayed growth inhibition similar to that of the widely used chemotherapeutic agent, cisplatin. In our previous study, ferrocene-appended organotin compounds were used to catalyse the oxidation of nicotinamide-adenine dinucleotide (NADH), leading to the accumulation of reactive oxygen species (ROS) and inducing A549 tumour cell apoptosis and oncosis [19]. These results indicate that ferrocene-based heteronuclear metal complexes display more excellent cytotoxic activity against the cancer cell lines compared with the ferrocene monomer, providing guidance regarding the design of metal anticancer drugs.

Iridium(III) (Ir^{III}) complexes have been rapidly developed as the effective substitutes for platinum anticancer drugs because of their special anticancer mechanisms, including favourable biocatalysis performance (Catalyze the oxidation of NADH, leading to production of ROS) and as various proteins inhibitors [20-22]. Among them, half-sandwich Ir^{III} complexes, generally described as $[(\eta^5\text{-Cp}^*)\text{Ir}(\text{L}^{\wedge}\text{L})\text{X}]\text{Z}$, have attracted more attention because of their favourable anticancer activity [23,24]. Interestingly, each part has a certain effect on the anticancer activity of these complexes, and the rational design has achieved success in the development of these complexes [3]. Cyclopentadienyl or its phenyl and biphenyl derivatives (Cp^*) occupy three coordination sites at the octahedral metal center and provide to the metal a lipophilic protecting face. The dentate ligand ($\text{L}^{\wedge}\text{L}$) and the leaving group (X, usually chlorine) occupy the remaining three coordination sites, which endow the whole complex with hydrophilic properties. Therefore, precise regulation between the lipophilic cyclopentadienyl derivative and the other coordinated ligands can effectively control the solubility, the ligand-exchange kinetics and the stability of these complexes [25]. Of course, the size and coordination ability of the counter ions (Z, usually PF_6^-) also has a significant influence on the chemical reactivity and anticancer activity of these complexes [26].

Multinuclear or heteronuclear metal complexes differ from the traditional metal complex monomers and have shown good application potential for treatment [27]. Considering the advantage of ferrocene derivatives and half-sandwich iridium(III) complexes in the field of anticancer, Fe(II)-Ir(III) heteronuclear metal complexes (**Fe-Ir1**~**Fe-Ir4**, Scheme 1) were prepared and characterised in this paper. An MTT (3-(4,5-dimethylthiazol-2-yl) -2,5-diphenyltetrazolium bromide) assay indicated that these complexes had better anticancer activity than the monomers of ferrocene-bipyridine pro-ligands (**L1** and **L2**, Scheme 2) and half-sandwich Ir^{III} bipyridine complexes (**5** and **6**, Scheme S1), particularly those with a *cis*-configurational ones (**2** and **4**). We also investigated the intracellular tissue targeting and the anticancer mechanism of these complexes. The results indicated that Fe(II)-Ir(III) heteronuclear metal complexes had potential as anticancer agents for further evaluation.



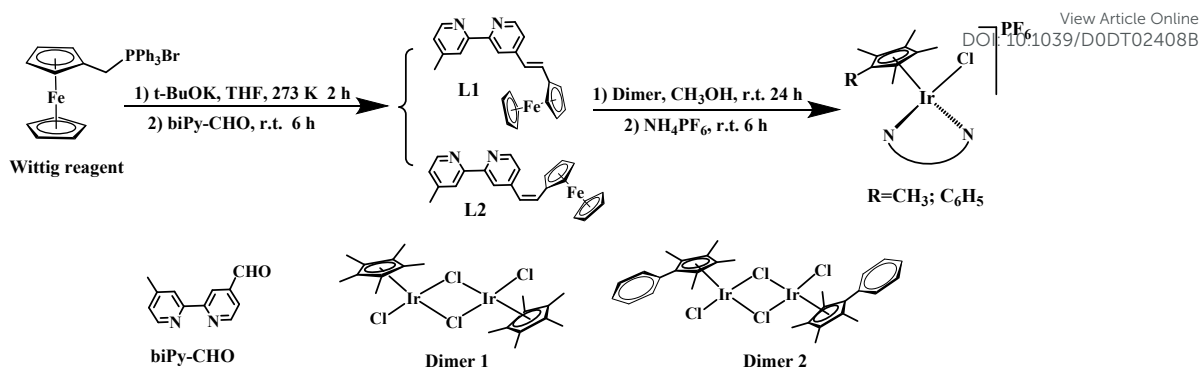
View Article Online
DOI: 10.1039/D0DT02408B

Scheme 1 Structures of designed Fe(II)-Ir(III) heteronuclear metal complexes, non-energy-dependent cellular uptake mechanism, targeted and damaged lysosome, led to the decrease of mitochondrial membrane potential (MMP) and the increase of reactive oxygen species (ROS), eventually induced apoptosis.

2 Results and discussion

2.1 Synthesis and general aspects

Fe(II)-Ir(III) heteronuclear metal complexes were obtained by the reaction of $[(\eta^5\text{-C}_5\text{Me}_5)\text{IrCl}_2]_2$ (Dimer **1**) or $[(\eta^5\text{-C}_5\text{Me}_4\text{C}_6\text{H}_5)\text{IrCl}_2]_2$ (Dimer **2**) with the corresponding ferrocene-modified bipyridine (N^N) bidentate ligands (**L1** and **L2**), **Scheme 2**. N^N-bidentate ligands (**L1** and **L2**) were obtained by the interaction of 4-formyl-4'-methyl-2,2'-bipyridine (biPy-CHO) and ferrocene methyl triphenylphosphine hydrobromate through the classical Wittig reaction and purified by column chromatography [28]. The *trans*- and *cis*-spatial configurations were confirmed by the hydrogen nuclear magnetic resonance (^1H NMR) spectra (**Fig. S1**), hydrogen atoms of the olefin were shown in the range of 6.4 ppm to 6.8 ppm with the coupling constant of 16.1 Hz and 12.0 Hz, respectively [29]. Complexes were synthesized and isolated as hexafluorophosphate in good yields (>85%), and fully characterised by NMR spectra (**Figs. S3** and **S4**), electrospray ionization mass spectra (ESI-MS, **Fig. S5**) and elemental analysis. Hydrogen atoms on the methyl of cyclopentadiene were shown in the range of 1.6 ppm to 1.8 ppm, and that of bipyridine changed from 2.6 ppm to 3.4 ppm. Hydrogen atoms on ferrocene were shown in the range of 4.2 ppm to 4.9 ppm, and others on pyridine and benzene appear in the range of 6.3 ppm to 8.9 ppm. The methyl carbon atoms of bipyridine were shown in 21.2~21.5 ppm, and which on Cp* were at 8.4~9.8 ppm in ^{13}C NMR spectra. The carbon atoms of ferrocene units listed in the range of 68.5~82.2 ppm. The results of ESI-MS were consistent with the theoretically calculated values (loss of PF_6^- or Cl^-).



Single crystals of **Fe-Ir1** suitable for X-ray diffraction analysis were obtained by slow diffusion of *n*-hexane into a saturated solution of dichloromethane. Crystal structure was shown in [Fig. 1](#), crystallographic data and selected bond length and angles were listed in [Tables S1](#) and [S2](#). Obviously, **Fe-Ir1** shows expected *trans*-configuration. In addition, metal iridium cell can be described as a “three-leg piano-stool” geometry [3], and ferrocene unit exhibit a superimposed configuration. Around the central iridium ion, the distance of Ir-Cl is longest, which is consistent with the conclusion that Ir-Cl bond is the active center for half-sandwich structural iridium(III) complexes [30].

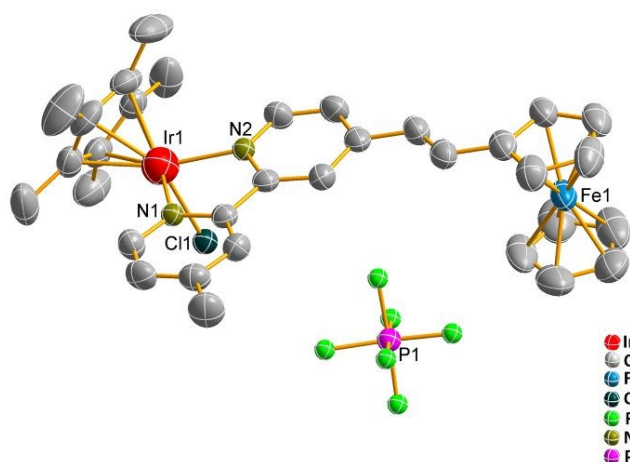


Fig. 1 X-ray crystal structure of **Fe-Ir1**. The thermal ellipsoids drawn at the 50% probability level (H atoms were omitted for clarity).

2.2 Cell cytotoxicity assay

The anticancer activity of Fe(II)-Ir(III) heteronuclear metal complexes against A549 (lung cancer cells) and HeLa (cervical cancer cells) cell lines was determined using the MTT (3-(4,5-dimethylthiazol-2-yl)-2,5-diphenyltetrazolium bromide) assay after 24 h treatment. Cisplatin, widely used clinically, was included as a control. The IC₅₀ values (concentration at which 50% of the cell growth is inhibited) are listed in [Table 1](#). As shown, compared with the basic ferrocene-appended bipyridine pro-ligands (**L1** and **L2**) and simple half-sandwich Ir^{III} bipyridine complexes (**Ir5** and **Ir6**, [Scheme S1](#)), Fe(II)-Ir(III) heteronuclear metal complexes exhibited better antitumor activity under the same conditions, the best of which (**Fe-Ir4**) showing almost 5-fold higher activity than cisplatin against A549 cells. These results indicate that

combining the ferrocene monomer and metal iridium(III) complex monomer can effectively improve the overall anticancer activity, particularly when they are connected through the *cis*-configuration olefin. However, the cytotoxicity of these complexes towards human lung epithelial cells (BEAS-2B, human normal cells) was also high under the same conditions, and no significant selectivity existed between normal cells and tumour cells. However, this favourable antitumor activity provided a structural foundation for the further design and optimization of such compounds.

View Article Online
DOI: 10.1039/D0DT02408B

Table 1 IC₅₀ values of target complexes, ferrocene-modified bipyridine pro-ligands (**L1**, **L2**) and cisplatin against A549, HeLa and BEAS-2B cell lines determined by MTT assay after 24 h.

Complex	IC ₅₀ (μM)		
	A549	Hela	BEAS-2B
Fe-Ir1	30.34±4.88	21.42±0.81	33.48 ± 0.41
Fe-Ir2	19.90±0.66	13.90±0.79	23.66 ± 0.72
Fe-Ir3	6.70±0.40	7.42±0.41	8.06 ± 0.03
Fe-Ir4	4.81±0.27	5.51±0.10	7.32 ± 0.42
Ir5	> 100	> 100	> 100
Ir6	> 100	> 100	> 100
L1	92.91±1.32	> 100	> 100
L2	> 100	> 100	> 100
Cisplatin	21.32±1.71	7.52±0.21	38.40±2.83

Obviously, the anticancer activity of *cis*-configurational complexes is higher than that of the corresponding *trans*-configurational one (**Fe-Ir2** > **Fe-Ir1**; **Fe-Ir4** > **Fe-Ir3**) with the evidence of the lower IC₅₀ values, respectively. To understand these, quantum chemical computation was used to evaluate after adequately considering the crystal structure of **Fe-Ir1**. The data of natural population analysis (NPA) for central atom (Ir) and the leaving group (Cl) and Wiberg bond order of Ir-Cl bond in **Fe-Ir1** and **Fe-Ir2** were analysed by density functional theory (DFT) calculation at the B3LYP/6-31G(d, p) (C, H, N, Cl)/SDD (Ir) level. **Fe-Ir1** exhibit a little larger Wiberg bond order (0.6217) than **Fe-Ir2** (0.6187). Meanwhile, the values of NPA charge population for Cl in **Fe-Ir1** and **Fe-Ir2** are -0.343 and -0.327, however, which for Ir are almost the same (0.173 and 0.172, respectively). Although the N^N bidentate pro-ligand (**L1**) containing *trans*-configurational alkene has the smaller bond angles (Table S3), the electron cloud configuration of front orbitals, HOMO (Highest Occupied Molecular Orbital) and LUMO (Lowest Unoccupied Molecular Orbital), shows the combination of ferrocene and bipyridine does not effectively improve the conjugation of the whole pro-ligands (HOMOs are mainly localized on ferrocene and olefin; LUMOs are mainly localized on Ir, Cl, bipyridine unit and olefin; Fig. S6), which have almost the similar electron-donating abilities and contribute to the similar charges in the central iridium ions. Therefore, the lower the charge of Cl⁻, the stronger the Ir-Cl bond, and the worse the anticancer activity of **Fe-Ir1** [30]. Additionally, dimer **2**-based complexes (**Fe-Ir3** and **Fe-Ir4**) showed better antitumor activity than the corresponding dimer **1**-based one. The oil-water distribution coefficients (log*P*_{o/w}) were determined by UV-visible (UV-vis) spectra, and the values were 0.38 and 0.61 for **Fe-Ir1** and **Fe-Ir3**, respectively. This conclusion indicates the increase of lipid solubility is beneficial to the improvement of anticancer activity for these complexes. All these provide the basic premise for further design and optimization of such complexes.

Hydrolysis of M–Cl bonds can represent an activation step for half-sandwich transition metal anticancer complexes. M–OH₂ aqua complexes are usually more reactive than the corresponding chloride complexes [3,30]. The hydrolysis characteristic of **Fe-Ir3** and **Fe-Ir4** in 20% CH₃OH/80% H₂O (v/v) solution at 298 K over 8 h was monitored by UV-vis absorption spectra (Fig. S7). The presence of methanol ensured the solubility of these complexes. Time dependence of the formation of the aqua adducts of complexes was fitted to pseudo first-order kinetics (Fig. S8). The values of hydrolysis rate constants are 0.00128 min⁻¹ and 0.00305 min⁻¹, and the half-lives of hydrolysis are 541.5 min and 227.3 min for **Fe-Ir3** and **Fe-Ir4**, respectively. Fe(II)-Ir(III) heteronuclear metal complexes undergo a much slower hydrolysis, and the hydrolytic half-life of **Fe-Ir4** is about 2.5 times faster than that of **Fe-Ir3**, which helps **Fe-Ir4** to exhibit the better anticancer activity.

2.3 Cellular uptake and localization assay

Owing to the favourable anticancer activity against the A549 cell line, the subcellular localisation in A549 cells of these complexes was determined by using laser confocal microscopy. Lyso Tracker Red DND-99 (LTRD) and Mito Tracker Deep Red (MTDR) were employed as fluorescent probes for the lysosomes and mitochondria, respectively [31]. At an appropriate fluorescence emission (no conflict with the fluorescent probe of Lyso Tracker Red DND-99 and Mito Tracker Deep Red, Fig. S9), **Fe-Ir3** and **Fe-Ir4** were shown to effectively accumulate in lysosomal tissues with the Pearson's colocalization coefficients of 0.72 and 0.76 over 2 h (Fig. 2). However, the Pearson's colocalisation coefficients for mitochondria targeting were 0.11 and 0.17, respectively. This result indicates that Fe(II)-Ir(III) heteronuclear metal complexes are mainly target lysosomes *in vivo*. Additionally, these complexes do not cause abnormal cell death immediately, making them convenient for tracking real-time changes in lysosomal morphology.

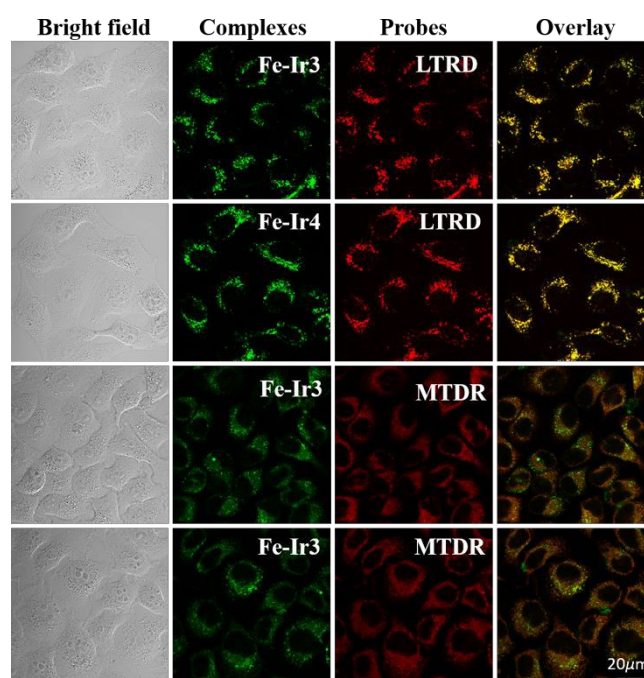


Fig. 2 Determination of intracellular localization of **Fe-Ir3** and **Fe-Ir4** in A549 cells by laser confocal microscopy. A549 cells were incubated with LTRD and MTDR, and then exposed to **Fe-Ir3** and **Fe-Ir4** ($1.0 \times IC_{50}$). LTRD was excited at 594 nm and collected at 600-660 nm.

MTDR was excited at 644 nm and collected at 660-720 nm. Complexes were excited at 405 nm and the emission was collected at 420-500 nm. Scale bar: 20 μm .

Lysosomes, which are acidic intracellular organelles (pH=3.5-5.5), can destroy biological macromolecules [32]. Widespread disruption of lysosomal integrity can lead to the release of cathepsins and other hydrolases from the lysosomal lumen into the cytosol, thus initiating apoptosis [33]. Acridine orange (AO), with red/green fluorescence in the lysosomes/cytosol, is typically utilised as a probe to determine the integrity of lysosomes. A549 cells were exposed to **Fe-Ir3** and **Fe-Ir4** ($1.0 \times \text{IC}_{50}$ and $3.0 \times \text{IC}_{50}$) for 2 h, and then stained with AO ($5 \mu\text{M}$), Figs. 3 and S10. Compared with the control, an obviously decrease in red fluorescence was observed in the presence of these complexes ($1.0 \times \text{IC}_{50}$), and obvious lysosomal damage was found at a concentration of $3.0 \times \text{IC}_{50}$. This suggests that Fe(II)-Ir(III) heteronuclear metal complexes may accumulate in lysosomes, followed by disruption of lysosomal integrity and eventually induction of cell death.

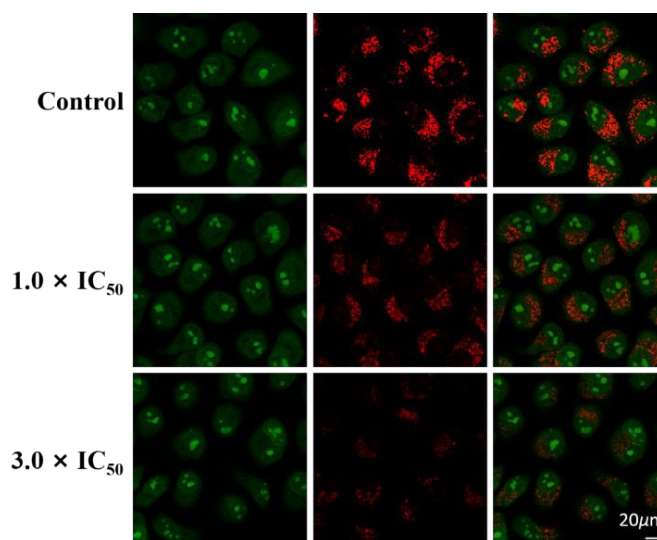


Fig. 3 Lysosomal damage in A549 cells caused by **Fe-Ir4** with AO ($5.0 \mu\text{M}$) staining at $37 \text{ }^\circ\text{C}$ for 15 min. Emission was collected at $510 \pm 20 \text{ nm}$ (green) and $625 \pm 20 \text{ nm}$ (red) upon excitation at 488 nm. Scale bar: 20 μm .

A good intracellular uptake mechanism is beneficial for improving drug activity. After treatment with **Fe-Ir3** and **Fe-Ir4** at 277 K and 310 K and preincubation with chlorocyanochlorophenyl (CCCP, metabolic inhibitor, $10 \mu\text{M}$) and chloroquine (endocytosis modulator, $50 \mu\text{M}$) for 2 h, A549 cells were evaluated to determine the cellular uptake mechanisms (Fig. S11). Energy-dependent mechanisms (including active transport and endocytosis) and non-energy-dependent mechanisms (including passive transport and free diffusion) are the two main cellular uptake mechanisms of organometallic drugs [34]. As shown, there was almost no change compared with the control, indicating that Fe(II)-Ir(III) heteronuclear metal complex entering cell follows a non-energy-dependent pathway [35].

2.4 Anticancer mechanism assay

Apoptosis refers to the autonomous and orderly death of cells controlled by genes in order to maintain internal environment stability, and most transition metal anticancer drugs can clear

tumour cells by inducing apoptosis [36]. In order to investigate whether Fe(II)-Ir(III) heteronuclear metal complexes could induce apoptosis, A549 cells were stained with annexin V-FITC/PI (propidium iodide) and then hatched with **Fe-Ir3** and **Fe-Ir4** at the concentrations of $1.0 \times IC_{50}$, $2.0 \times IC_{50}$ and $3.0 \times IC_{50}$ for 24 h, followed by flow cytometry analysis (Fig. 4 and Tables S4-S5). **Fe-Ir3** and **Fe-Ir4** induced the apoptosis of A549 cell in a dose-dependent manner, mainly in the late apoptosis phase. The percentage of late apoptosis cells increased from 15.6% and 21.3% to 25.5% and 30.1% when the concentrations of **Fe-Ir3** and **Fe-Ir4** were changed from $1.0 \times IC_{50}$ to $3.0 \times IC_{50}$, respectively. Additionally, >94% of A549 cells survived in the control groups under the same conditions. This confirms that Fe(II)-Ir(III) heteronuclear metal complexes can lead to tumour cell death via apoptosis.

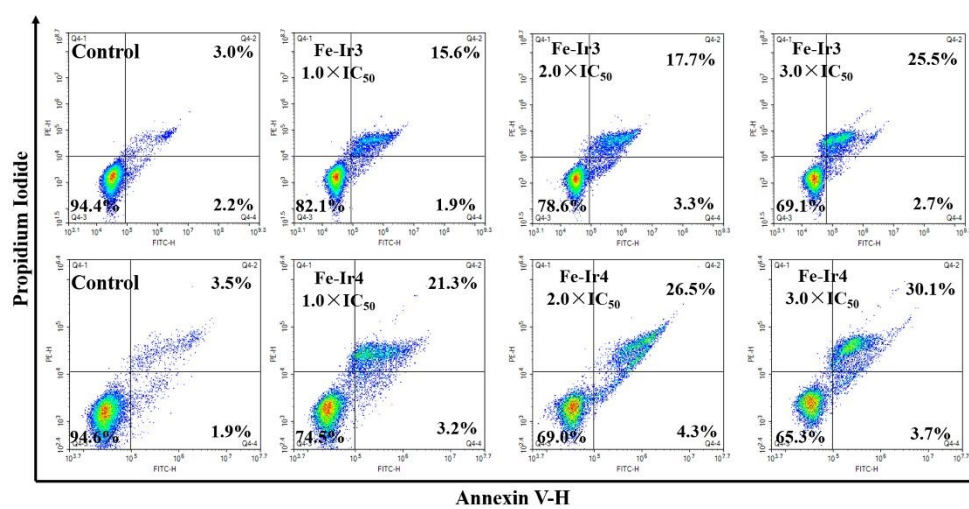
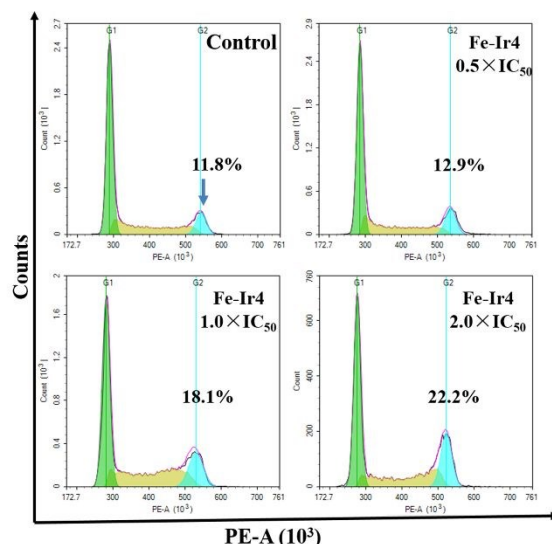


Fig. 4 Flow cytometric quantification of annexin V-FITC and propidium iodide (PI) double-labeled A549 cells treated with **Fe-Ir3** and **Fe-Ir4** for 24 h.

Generally, organometallic anticancer complexes could cause a functional decline by disrupting the cell cycle and exert their effects. [37] To investigate the effect of Fe(II)-Ir(III) heteronuclear metal complexes on tumour cell cycle arrest, A549 cells, stained by PI, were exposed to **Fe-Ir3** and **Fe-Ir4** at the concentration of $0.5 \times IC_{50}$, $1.0 \times IC_{50}$ and $2.0 \times IC_{50}$ for 24 h and analysed by flow cytometry. As shown in Fig. 5 and Tables S6-S7, the percentages of cells in the G2/M phase increased from 12.9% to 22.2% when the concentration changed from $0.5 \times IC_{50}$ to $2.0 \times IC_{50}$ for **Fe-Ir4**, however, which for **Fe-Ir3** only increased by 2.0%. More important, though less visible, is the contribution to blocking the cell cycle.



View Article Online
DOI: 10.1039/D0DT02408B

Fig. 5 Distribution of A549 cells labeled with PI after incubation with **Fe-Ir4** ($0.5 \times IC_{50}$, $1.0 \times IC_{50}$ and $2.0 \times IC_{50}$) for 24 h. The marked numbers were the percentages of cells in the G2/M phase.

Additionally, mitochondria, the source of energy or adenosine triphosphate (ATP) in cells, play a unique role in the process of apoptosis. [38] The decrease of mitochondrial membrane potential (MMP) is a vital signal in the early apoptotic process. [39] JC-1 (5,5,6,6'-tetrachloro-1,1',3,3' tetraethyl benzimidazolyl carbocyanine iodide), an ideal fluorescent probe for detecting MMP (the high and low MMP corresponding to the red and green fluorescence in the aggregate and monomer state), was utilised to clarify whether apoptosis induced through destroying mitochondrial homeostasis and estimated by flow cytometry [40], Fig. S12. As shown, a dose-dependent decline of MMP occurs in A549 cells induced by **Fe-Ir3** and **Fe-Ir4**. Compared with the negative control, the population of mitochondrial membrane depolarized cells increase by 8.1% and 21.8% for **Fe-Ir3** and **Fe-Ir4** at the concentration of $2.0 \times IC_{50}$, respectively. It's not hard to see that although these complexes do not target mitochondria, widespread lysosomal damage verified by laser confocal testing results in the release of hydrolases from the lysosomal lumen to the cytosol, which directly leads to the mitochondrial dysfunction and eventually apoptosis.

Reactive oxygen species (ROS) are mainly produced and stored in the mitochondria, and increased intracellular ROS levels may induce apoptosis [41,42]. Oxidant-sensitive DCFH-DA (2,7-dichlorodi-hydrofluorescein diacetate), a fluorescent probe, was used to monitor the intracellular ROS levels in A549 cells using flow cytometry, Fig. S13. The ROS levels in A549 cells show a dose-dependent increase as the concentrations of **Fe-Ir3** and **Fe-Ir4** were increased from $0.25 \times IC_{50}$ to $0.5 \times IC_{50}$ after 24 h exposure. Compared with the negative control, intracellular ROS levels showed 1.23/1.44-fold increases for **Fe-Ir3/Fe-Ir4** when the concentration was $0.5 \times IC_{50}$, respectively. Additionally, NADH (the reduced state of nicotinamide adenine dinucleotide) plays a key role in regulating energy production in mitochondria.⁴⁵ Transition metal complexes can catalyse the oxidation of NADH and lead to the accumulation of ROS (1O_2), exerting an antitumor mechanism of oxidation [43]. The UV-vis spectrum was utilised to investigate the interaction between complexes and NADH in 10% $CH_3OH/90\%$ H_2O (v/v) at 298 K at different time points, Fig. 6. The intensity of absorbance at 339 nm (the maximum absorbance of NADH) and 259 nm (the maximum absorbance of NAD^+ , oxidation state of NADH, loss of hydrogen catalyzed by organometallic compounds) significantly decreased and

increased over time, respectively [44]. These changes were well-reflected by the turnover numbers (TONs, the change ratio at 339 nm). **Fe-Ir4** showed a higher TON than **Fe-Ir3**, indicating that *cis*-configurational complexes possess the better biocatalytic performance relative to *trans*-configurational complexes. Overall, widespread lysosomal damage leads to apoptosis, which can be revealed by a decrease in mitochondrial membrane potential, increase in intracellular reactive oxygen species (Scheme 1), catalytic acceleration of NADH oxidation, and an antitumor mechanism of oxidation.

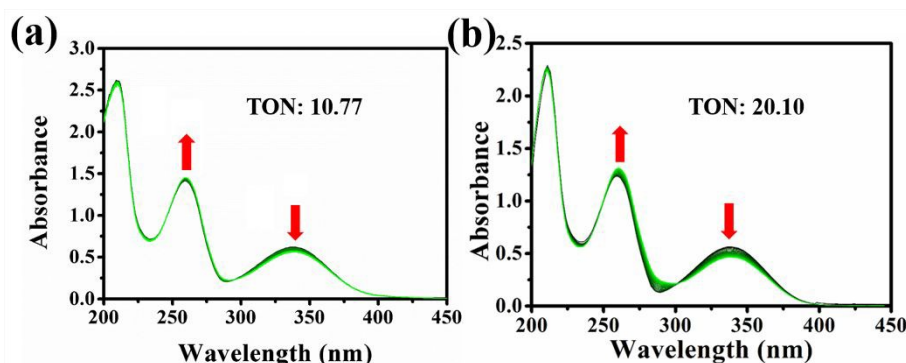


Fig. 6 UV-vis spectra of NADH (100 μ M) with **Fe-Ir3** (a) and **Fe-Ir4** (b) in 10% $\text{CH}_3\text{OH}/90\%$ H_2O (v:v) over 8 h at 298 K. The arrows show the changes over time.

2.5 Transport mechanism assay

Human serum albumin (HSA) is the most abundant carrier protein in the human plasma, which can bind a variety of substrates, including hormones, metal cations and most therapeutic drugs. Bovine serum albumin (BSA) is usually utilised as a model to investigate the transport mechanism of organometallic anticancer drugs due to the advantages of resemblance to HSA, abundance, stability, ease of purification, *etc.* [45] Therefore, in this study, UV-vis spectra and fluorescence spectra were used to determine the binding mechanism between these complexes and serum albumin. As shown in Figs. 7a and S14a, a significant reduction is found at 227 nm (the UV-vis absorption of BSA) along with a red shift (~ 7 nm, induced by the polar solvent) with the increase of **Fe-Ir3** and **Fe-Ir4**, which indicates that Fe(II)-Ir(III) heteronuclear metal complexes can change the conformation of BSA, reduce the content of the α -helix structure and loosen the conformation of the protein [46]. In addition, a slight change (increase and decrease for **Fe-Ir3** and **Fe-Ir4**, respectively) without any shift at 278 nm suggest that complexes can interact with BSA and closely relate to the microenvironment of aromatic acid residues in BSA. Among them, tyrosine and tryptophan, two main aromatic acid residues, can be reflected by the wavelength interval of $\Delta\lambda = 15$ nm and 60 nm through synchronous fluorescence, respectively [47]. As shown in Figs. 7C, 7d, S14c and S14d, the fluorescence intensity for BSA at 291 nm and 285 nm ($\Delta\lambda = 15$ nm and 60 nm, respectively) weaken quickly with the increase of complexes. Additionally, a minor red shift (~ 3 nm) occurs at 285 nm ($\Delta\lambda = 60$ nm) at the investigated concentration range, however, almost no change occurred at the wavelength of $\Delta\lambda = 15$ nm. The results indicated that the conformation of BSA was changed, and the polarity around the tryptophan residues increased [48].

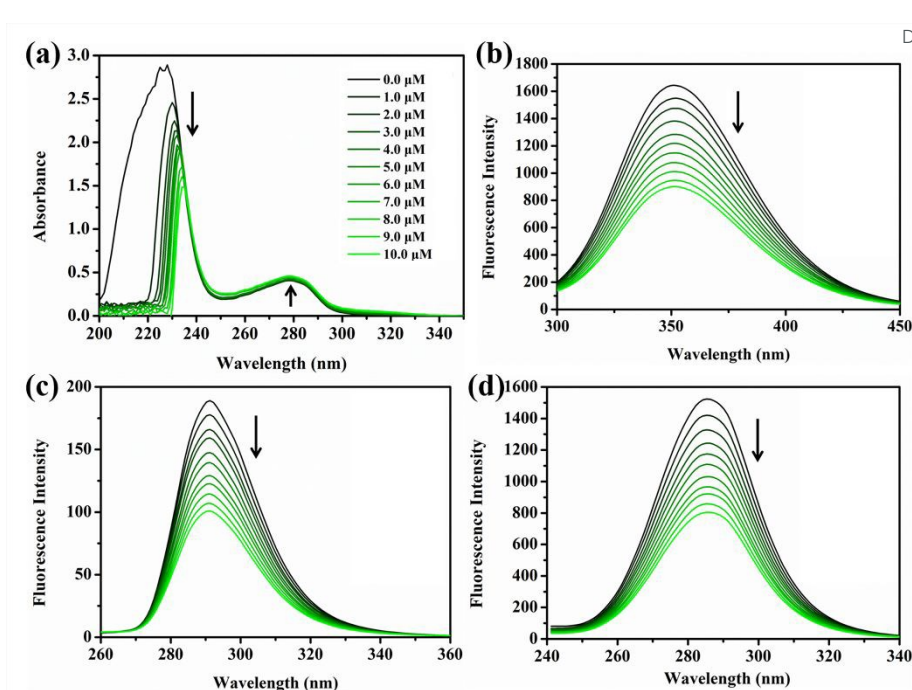


Fig. 7 (a) UV-vis spectra of BSA in 5 mM Tris-HCl/10 mM NaCl buffer solution (pH = 7.2) with the increase of **Fe-Ir3** (0-10 μM). The arrows show the direction of changes in absorbance; (b) Fluorescence spectra of BSA (5 μM ; $\lambda_{\text{ex}} = 280 \text{ nm}$; $\lambda_{\text{em}} = 350 \text{ nm}$) in the absence and presence of **Fe-Ir3** (0-10 μM); Synchronous spectra of BSA (5 μM) in the presence of increasing amounts of **Fe-Ir3** (0-10 μM) with a wavelength of $\Delta\lambda = 15 \text{ nm}$ (c) and $\Delta\lambda = 60 \text{ nm}$ (d).

The interaction mechanism between **Fe-Ir3/Fe-Ir4** and BSA was further investigated by the fluorescence quenching phenomenon of BSA [49], Figs. 7b and S14b. A significant quenching at 343 nm (the fluorescent emission peak of BSA) was found with the increase of **Fe-Ir3** and **Fe-Ir4**. The Stern–Volmer quenching constant (K_{sv}) and quenching rate constant (K_{q}) can be obtained through the classical Stern–Volmer equation (Figs. S15a and S15b). Dynamic mechanism and static mechanism are two main mechanism of fluorescence quenching [50]. As shown in Table 2, the values of K_{q} were $8.6 \times 10^{12} \text{ M}^{-1} \text{ s}^{-1}$ and $1.24 \times 10^{13} \text{ M}^{-1} \text{ s}^{-1}$ for **Fe-Ir3** and **Fe-Ir4**, respectively, which were almost one order of magnitude higher than that of a pure dynamic quenching mechanism ($< 2.0 \times 10^{12} \text{ M}^{-1} \text{ s}^{-1}$) [51]. This conclusion indicated that Fe(II)-Ir(III) heteronuclear metal complexes could interact with BSA abiding by a static quenching mechanism. Additionally, binding site number (n) and the binding constant (K_{b}) were further calculated through the Scatchard equation (Figs. S15c and S15d). Although the values of n (≈ 1) were almost the similar, **Fe-Ir4** exhibited the higher binding constant (K_{b}) than that of **Fe-Ir3**, which indicated that the introduction of *cis*-configurational olefin could decrease the steric hindrance between complex and BSA. This conclusion is consistent with that of toxicity test that **Fe-Ir2** and **Fe-Ir4** show the better anticancer activity than the corresponding *trans*-configurational ones. In summary, the stable combination with BSA suggested that BSA is expected to become an excellent carrier for delivery of anticancer agents in plasma.

Table 2 The values of K_{sv} , K_{b} , K_{q} and n for complexes **1** and **4** at 298 K.

K_{sv}	K_{q}	K_{b}	n
(10^5 M^{-1})	($10^{13} \text{ M}^{-1} \text{ s}^{-1}$)	(10^4 M^{-1})	

Fe-Ir3	0.86±0.05	0.86	5.64	1.15
Fe-Ir4	1.24±0.13	1.24	6.50	1.23

View Article Online
DOI: 10.1039/D0DT02408B

Conclusion

In this paper, four configuration-controlled Fe(II)-Ir(III) heteronuclear metal complexes were prepared and characterized. The combination of ferrocene monomer and half-sandwich Ir^{III} complex monomer effectively improved the anticancer activity of target complexes, especially for the *cis*-configurational one. **Fe-Ir4**, the best of these complexes, were almost five times of cisplatin towards A549 cells under the same conditions. Laser confocal confirms complexes enter cells followed a non-energy-dependent mechanism, accumulate in lysosomes and induce the lysosomal damage, and lead to apoptosis. Complexes could decrease the mitochondrial membrane potential, disturb the cell cycle at G2/M phase, catalyze the oxidation of NADH and improve the levels of intracellular ROS, provide an anticancer mechanism of oxidation. Above all, Fe(II)-Ir(III) heteronuclear metal complexes may be a promising strategy for constructing potential organometallic anticancer therapeutic platform.

3 Experimental section

3.1 General information

Iridium trichloride hydrated, 1,2,3,4,5-pentamethyl-cyclopentadiene (95%), Phenyl magnesium bromide (1.0 M in THF), 2,3,4,5-tetramethyl-2-cyclopentenone (95%), ferrocenecarboxaldehyde, 4,4'-dimethyl-2,2'-bipyridine, selenium dioxide, sodium borohydride, triphenylphosphine hydrobromate, potassium tert-butoxide, ammonium hexafluorophosphate and all kinds of organic solvents (methylene dichloride, methanol, tetrahydrofuran and 1,4-dioxane *etc.*) were purchased from Rhea biotechnology co. LTD. For the biological experiments, DMEM medium, fetal bovine serum, penicillin/streptomycin mixture and trypsin/EDTA were purchased from Sangon Biotech. A549 (lung cancer cells) and Hela (cervical cancer cell) were obtained from Shanghai Institute of Biochemistry and Cell Biology (SIBCB). The appropriate dimer of iridium (Dimer **1** and Dimer **2**) were prepared according to literature procedures [50].

NMR spectra were obtained on Bruker DPX 500 spectrometers instrument, with the chemical shifts reported in ppm using tetramethylsilane (TMS) as an internal standard. Mass spectrum (MS) was measured on a Waters Q-TOF MicroTM mass spectrometer. Elemental analysis was performed on a VarioMICRO CHNOS elemental analyzer. UV-vis spectra and fluorescence spectra were collected on a PERSEE TU-1901 UV spectrometer and Hitachi F-4600 fluorescence spectrophotometer, respectively. Induction of apoptosis, cell cycle and mitochondrial membrane potential (MMP) determination were carried out by an ACEA Novocyte2040R flow cytometry. Viability assay (MTT) was measured using a Perlong DNM-9606 microplate reader at an absorbance of 570 nm. Cell uptake and cellular localization were carried out on a Carl Zeiss AG */LSM/880NLO two photon laser Scanning microscope.

3.2 Synthesis of ferrocene-modified bipyridine pro-ligands (L1-L2)

L1 and **L2** were synthesized by the classical Wittig reaction [28]: Ferrocene methyl triphenylphosphine hydrobromate (0.98 g, 1.82 mmol) was added into a 100 mL Schlenk flask under nitrogen. Anhydrous tetrahydrofuran (20 mL) was added to above flask and cooled down to 273 K. Tetrahydrofuran solution (10 mL) of potassium tert-butoxide (0.68 g, 6.05 mmol) was added dropwise to above flask and stirred for 30 min at 273 K. Then, tetrahydrofuran solution (10

mL) of 4-formyl-4'-methyl-2,2'-bipyridine (0.30 g, 1.51 mmol) was added and stirred at room temperature until 4-formyl-4'-methyl-2,2'-bipyridine was consumed completely (monitored by thin-layer chromatography). The reaction was terminated by ice water (50 mL). Extracted with ethyl acetate (30 mL×3), dried with anhydrous magnesium sulfate, and distilled under reduced pressure. The final product was purified by chromatograph on a silica gel column (petroleum ether: ethyl acetate =30:1 as eluent). The ¹H NMR, and ESI-MS of **L1** and **L2** were shown in Figs. S1-S2. The data were listed as follows:

L1: Yield: 0.26 g (45.1%). ¹H NMR (500 MHz, CDCl₃) δ 8.59 (t, *J* = 4.7 Hz, 2H), 8.43 (d, *J* = 20.9 Hz, 1H), 8.29 (s, 1H), 7.30 (dd, *J* = 8.5, 7.3 Hz, 2H), 7.17 (d, *J* = 4.6 Hz, 1H), 6.72 (d, *J* = 16.1 Hz, 1H), 4.55 – 4.50 (m, 2H), 4.39 – 4.34 (m, 2H), 4.16 (s, 5H), 2.46 (s, 3H). ESI-MS (*m/z*): calcd for C₂₃H₂₀N₂Fe, 380.1, found 381.2 [M+H]⁺.

L2: Yield: 0.21 g (36.5%). ¹H NMR (500 MHz, CDCl₃) δ 8.56 (dd, *J* = 4.9, 2.3 Hz, 2H), 8.40 (s, 1H), 8.30 (s, 1H), 7.36 (s, 1H), 7.18 (d, *J* = 4.5 Hz, 1H), 6.55 (d, *J* = 11.9 Hz, 1H), 6.41 (d, *J* = 12.0 Hz, 1H), 4.23 (s, 4H), 4.14 (s, 5H), 2.47 (s, 3H). ESI-MS (*m/z*): calcd for C₂₃H₂₀N₂Fe, 380.1, found 381.2 [M+H]⁺.

3.3 Synthesis of Fe(II)-Ir(III) heteronuclear metal complexes (Fe-Ir1 ~ Fe-Ir4)

The general synthesis method is as follows: Dimer of iridium (Dimer **1**/Dimer **2**, 39.8 mg/46.0 mg, 0.050 mmol) and ferrocene-modified bipyridine (**L1** and **L2**, 38.0 mg, 0.10 mmol) were added into a 100 mL Schlenk flask under nitrogen, and added methanol (30 mL) and stirred at ambient temperature overnight. Ammonium hexafluorophosphate (65.2 mg, 0.40 mmol) was added into the mixture and stirred for 6 h. The solvent was removed in vacuum and recrystallized from dichloromethane and *n*-hexane. The ¹H NMR, ¹³C NMR, ESI-MS and elementary analysis of complexes are shown in Figs. S3-S5. The data were listed as follows:

Fe-Ir1: Yield: 81.8 mg (92.1%). ¹H NMR (500 MHz, CDCl₃) δ 8.60 – 8.44 (m, 2H), 8.35 (d, *J* = 20.7 Hz, 2H), 7.53 (d, *J* = 15.2 Hz, 1H), 7.45 (d, *J* = 13.0 Hz, 2H), 6.62 (d, *J* = 14.0 Hz, 1H), 4.83 (s, 2H), 4.61 (s, 2H), 4.34 (s, 5H), 2.66 (s, 3H), 1.67 (s, 15H). ¹³C NMR (126 MHz, d⁶-DMSO) δ 155.41, 155.21, 152.77, 152.18, 151.65, 149.03, 139.10, 129.84, 125.38, 125.05, 121.24, 119.32, 89.21, 81.17, 71.21, 69.97, 68.58, 21.30, 8.63. ESI-MS (*m/z*): calcd for C₃₃H₃₅N₂ClFeIr, [M-PF₆]⁺, 743.147, found 743.097; calcd for C₃₃H₃₅N₂FeIr, [M-PF₆-Cl]²⁺, 708.178, found 708.125. Elemental analysis: calcd (%) for C₃₃H₃₅N₂ClFeIr: C, 44.63; H, 3.97; N, 3.15; found: C, 44.78.; H, 4.04; N, 3.11.

Fe-Ir2: Yield: 81.0 mg (91.2%). ¹H NMR (500 MHz, CDCl₃) δ 8.58 (d, *J* = 4.5 Hz, 1H), 8.50 (d, *J* = 5.5 Hz, 1H), 8.26 (s, 1H), 7.97 (s, 1H), 7.67 (d, *J* = 4.9 Hz, 1H), 7.50 (d, *J* = 4.2 Hz, 1H), 6.73 (d, *J* = 10.3 Hz, 1H), 6.43 (d, *J* = 11.5 Hz, 1H), 4.42 (dd, *J* = 29.5, 15.1 Hz, 4H), 4.25 (s, 5H), 2.63 (s, 3H), 1.68 (s, 15H). ¹³C NMR (126 MHz, d⁶-DMSO) δ 155.40, 155.19, 152.77, 152.15, 151.62, 149.02, 139.10, 129.83, 125.34, 125.04, 121.19, 119.34, 89.20, 81.17, 71.21, 69.96, 68.57, 21.29, 8.62. ESI-MS (*m/z*): calcd for C₃₃H₃₅N₂ClFeIr, [M-PF₆]⁺, 743.147, found 743.076; calcd for C₃₃H₃₅N₂FeIr, [M-PF₆-Cl]²⁺, 708.178, found 708.096. Elemental analysis: calcd (%) for C₃₃H₃₅N₂ClFeIr: C, 44.63; H, 3.97; N, 3.15; found: C, 44.81.; H, 4.03; N, 3.13.

Fe-Ir3: Yield: 83.8 mg (88.2%). ¹H NMR (500 MHz, DMSO) δ 8.84 (s, 1H), 8.79 (s, 1H), 8.54 (d, *J* = 5.6 Hz, 1H), 8.46 (d, *J* = 5.7 Hz, 1H), 7.80 (d, *J* = 16.1 Hz, 1H), 7.73 (s, 1H), 7.65 (s, 1H), 7.50 (s, 5H), 6.93 (d, *J* = 15.9 Hz, 1H), 4.70 (s, 2H), 4.55 (s, 2H), 4.22 (s, 5H), 2.65 (s, 3H), 1.78 (d, *J* = 9.0 Hz, 6H), 1.69 (s, 6H). ¹³C NMR (126 MHz, d⁶-DMSO) δ 155.58, 155.34, 153.06, 151.32, 150.93, 150.91, 149.26, 139.49, 130.47, 129.91, 129.75, 129.43, 125.31, 125.20, 121.03,

119.78, 98.82, 87.32, 86.68, 82.15, 71.27, 69.98, 68.56, 21.30, 9.73, 8.55. ESI-MS (m/z): calcd for $C_{38}H_{37}N_2ClFeIr$, [M-PF₆]⁺, 805.162, found 806.240; calcd for $C_{38}H_{37}N_2FeIr$, [M-PF₆-Cl]²⁺, 770.194, found 771.304. Elemental analysis: calcd (%) for $C_{38}H_{37}N_2ClF_6PF_6FeIr$: C, 48.03; H, 3.93; N, 2.95; found: C, 48.32; H, 4.05; N, 2.91.

Fe-Ir4: Yield: 81.3 mg (85.6%). ¹H NMR (500 MHz, CDCl₃) δ 8.36 (d, J = 5.8 Hz, 1H), 8.30 – 8.26 (m, 2H), 7.99 (s, 1H), 7.58 (dd, J = 7.5, 1.9 Hz, 2H), 7.50 (t, J = 6.2 Hz, 4H), 7.36 (d, J = 5.8 Hz, 1H), 6.71 (d, J = 11.5 Hz, 1H), 6.40 (d, J = 11.7 Hz, 1H), 4.46 (s, 1H), 4.41 (s, 2H), 4.34 (s, 1H), 4.24 (s, 5H), 2.60 (s, 3H), 1.77 (d, J = 6.2 Hz, 6H), 1.73 (d, J = 1.3 Hz, 6H). ¹³C NMR (126 MHz, CDCl₃) δ 155.32, 155.15, 153.07, 150.10, 149.91, 149.68, 137.63, 130.32, 129.60, 129.44, 129.29, 128.60, 127.29, 124.97, 123.59, 121.69, 99.56, 99.41, 99.33, 86.77, 85.94, 81.81, 71.27, 69.98, 68.56, 21.47, 9.78, 9.76, 8.52, 8.48. ESI-MS (m/z): calcd for $C_{38}H_{37}N_2ClFeIr$, [M-PF₆]⁺, 805.162, found 805.167. Elemental analysis: calcd (%) for $C_{38}H_{37}N_2ClF_6PF_6FeIr$: C, 48.03; H, 3.93; N, 2.95; found: C, 48.31; H, 4.07; N, 2.92.

Acknowledgments

We thank the National Natural Science Foundation of China (21671118 and 21703118), the Taishan Scholars Program, the Student's Platform for Innovation and Entrepreneurship Training Program (2018A043) and High Performance Computing Center of Qufu Normal University for support.

Supporting Information

Details of the experimental section, [Scheme S1](#), [Figures S1–S15](#), and [Tables S1–S7](#).

Accession Codes

CCDC 1996137 contain the supplementary crystallographic data for this paper. These data can be obtained free of charge via www.ccdc.cam.ac.uk/data_request/cif, or by emailing data_request@ccdc.cam.ac.uk, or by contacting The Cambridge Crystallographic Data Centre, 12 Union Road, Cambridge CB2 1EZ, UK; fax: +441223 336033.

References

- [1] G. Gasser, I. Ott and N. Metzler-Nolte, Ferrocenes as potential chemotherapeutic drugs: Synthesis, cytotoxic activity, reactive oxygen species production and micronucleus assay, *J. Med. Chem.*, 2011, **54**, 3–25.
- [2] K. Henize and H. Lang, Ferrocene-beauty and function, *Organometallics*, 2013, **32**, 5623–5625.
- [3] Z. Liu and P. J. Sadler, Organometallic half-sandwich iridium anticancer complexes, *Acc. Chem. Res.*, 2014, **47**, 1174–1185.
- [4] C. Ornelas, Application of ferrocene and its derivatives in cancer research, *New J. Chem.*, 2011, **35**, 1973–1985.
- [5] R. L. Siegel, K. D. Miller, A. Jemal, Cancer statistics, 2020, *CA Cancer J. Clin.*, 2020, **70**, 7-30.
- [6] C. C. Konkankit, S. C. Marker, K. M. Knopf and J. J. Wilson, Anticancer activity of complexes of the third row transition metals, rhenium, osmium, and iridium, *Dalton Trans.*, 2018, **47**, 9934-9974.

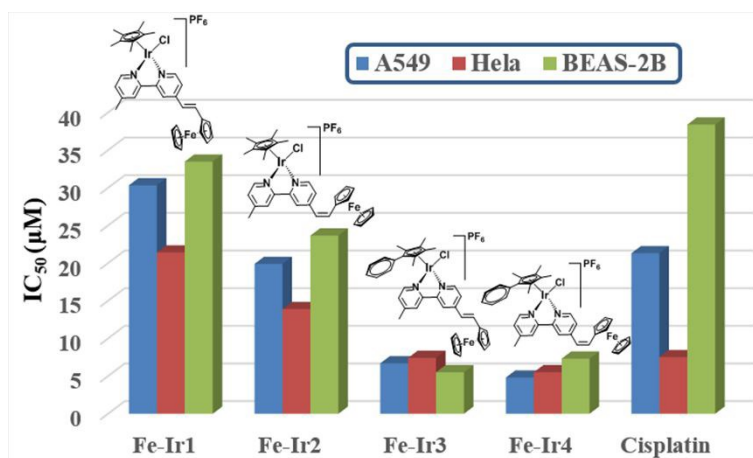
- [7] P. Zhang and H. Huang, Future potential of osmium complexes as anticancer drug candidates, photosensitizers and organelle-targeted probes, *Dalton Trans.*, 2018, **47**, 14841-14854. View Article Online
DOI: 10.1039/D0DT02408B
- [8] X. Wang, X. Wang, S. Jin, N. Muhammad and Z. Guo, Ferrocene-appended iridium(III) complexes: Configuration regulation, anticancer application, and mechanism research, *Chem. Rev.*, 2019, **119**, 1138-1192.
- [9] F. A. Larik, A. Saeed, T. A. Fattah, U. Muqadar and P. A. Channar, Recent advances in the synthesis, biological activities and various applications of ferrocene derivatives, *Appl. Organomet. Chem.*, 2017, **31**, 3664.
- [10] H. Z. S. Lee, O. Buriez, E. Labbe, S. Top, P. Pigeon, G. Jaouen, C. Amatore and W. K. Leong, Oxidative sequence of a ruthenocene-based anticancer drug candidate in a basic environment, *Organometallics*, 2014, **33**, 4940-4946.
- [11] A. Citta, A. Folda, A. Bindoli, P. Pigeon, S. Top, A. Vessieres, M. Salmain, G. Jaouen and M. P. Rigobello, Oxidative sequence of a ruthenocene-based anticancer drug candidate in a basic environment, *J. Med. Chem.*, 2014, **57**, 8849-8859.
- [12] M. Gormen, D. Plazuk, P. Pigeon, E. A. Hillard, M. A. Plamont, S. Top, A. Vessières and G. Jaouen, Facile synthesis and strong antiproliferative activity of disubstituted diphenylmethylidene ferrocenophanes on breast and prostate cancer cell lines, *Tetrahedron Lett.*, 2010, **51**, 118-120.
- [13] D. Osella, M. Ferrali, P. Zanello, F. Laschi, M. Fontani, C. Nervi and G. Cavigliolo, On the mechanism of the antitumor activity of ferrocenium derivatives, *Inorg. Chim. Acta*, 2000, **306**, 42-48.
- [14] G. Tabbi, C. Cassino, G. Cavigliolo, D. Colangelo, A. Ghiglia, I. Viano and D. Osella, Water stability and cytotoxic activity relationship of a series of ferrocenium derivatives. ESR insights on the radical production during the degradation process, *J. Med. Chem.*, 2002, **45**, 5786-5796.
- [15] K. Kowalski, P. Hikiş, L. Szczupak, B. Therrien and A. KocevaChyla, Anticancer and antibacterial activity studies of gold(I)-alkynyl chromones, *Eur. J. Med. Chem.*, 2014, **81**, 289-300.
- [16] A. Singh, I. Lumb, V. Mehra and V. Kumar, Ferrocene-appended pharmacophores: An exciting approach for modulating the biological potential of organic scaffolds, *Dalton Trans.*, 2019, **48**, 2840-2860.
- [17] X. Ge, S. Chen, X. Liu, Q. Wang, L. Gao, C. Zhao, L. Zhang, M. Shao, X. Yuan, L. Tian and Z. Liu, Ferrocene-appended iridium(III) complexes: Configuration regulation, anticancer application, and mechanism research, *Inorg. Chem.*, 2019, **58**, 14175-14184.
- [18] J. Rajput, J. R. Moss, A. T. Hutton, D. T. Hendricks, C. E. Arendse and C. Imrie, Discrete metal complexes from N-heterocyclic ferrocenes: Structural diversity by ligand design, *J. Organomet. Chem.*, 2004, **689**, 1553-1568.
- [19] J. Li, X. Liu, H. Zhang, X. Ge, Y. Tang, Z. Xu, L. Tian, X. Yuan, X. Mao and Z. Liu, Ferrocenyl-triphenyltin complexes as lysosome-targeted imaging and anticancer agents, *Inorg. Chem.*, 2019, **58**, 1710-1718.
- [20] S. Chen, X. Liu, J. Huang, X. Ge, Q. Wang, M. Yao, Y. Shao, T. Liu, X. Yuan, L. Tian and Z. Liu, Triphenylamine/carbazole-modified ruthenium(II) Schiff base compounds: synthesis, biological activity and organelle targeting, *Dalton Trans.*, 2020, **49**, 8774-8784.

- [21] J. J. Conesa, A. C. Carrasco, V. Rodriguez-Fanjul, Y. Yang, J. L. Carraxcosa, P. Cloetens, E. Pereiro and A. M. Pizarro, Unambiguous Intracellular Localization and Quantification of a Potent Iridium Anticancer Compound by Correlative 3D Cryo X-Ray Imaging, *Angew. Chem. Int. Ed.*, 2020, **59**, 1270-1278.
- [22] S. Parveen, M. Hanif, E. Leung, K. K. H. Tong, A. Yang, J. Astin, G. H. D. Zoysa, T. R. Steel, D. Goodman, S. Movassaghi, T. Söhnle, V. Sarojini, S. M. F. Jamieson and C. G. Hartinger, Anticancer organorhodium and -iridium complexes with low toxicity in vivo but high potency in vitro: DNA damage, reactive oxygen species formation, and haemolytic activity *Chem. Commun.*, 2019, **55**, 12016-12019.
- [23] X. Liu, S. Chen, X. Ge, Y. Zhang, Y. Xie, Y. Hao, D. Wu, J. Zhao, X. Yuan, L. Tian and Z. Liu, Dual functions of iridium (III) 2-phenylpyridine complexes: Metastasis inhibition and lysosomal damage, *J. Inorg. Biochem.*, 2020, **205**, 110983.
- [24] G. S. Yellol, A. Donaire, J. G. Yellol, V. Vasylyeva, C. Janiakb and J. Ruiz, Significant effects of counteranions on the anticancer activity of iridium(III) complexes, *Chem. Commun.*, 2013, **49**, 11533-11535.
- [25] G. Gupta, A. Garci, B. S. Murray, P. J. Dyson, G. Fabre, P. Trouillas, F. Giannini, J. Furrer, G. Süss-Fink and B. Therrien, Synthesis, molecular structure and cytotoxicity of molecular materials based on water soluble half-sandwich Rh(III) and Ir(III) tetranuclear metalla-cycles, *Dalton Trans.*, 2013, **42**, 15457–15463.
- [26] H. Zhang, L. Guo, Z. Tian, M. Tian, Sh. Zhang, Zh. Xu, P. Gong, X. Zheng, Jia. Zhao and Z. Liu, Electronic effects on reactivity and anticancer activity by half-sandwich *N, N*-chelated iridium(III) complexes, *Chem. Commun.*, 2018, **54**, 4421-4424.
- [27] C. M. Anderson, S. S. Jain, L. Silber, K. Chen, S. Guha, W. Zhang, E. C. McLaughlin, Y. Hu and J. M. Tanski, Synthesis and characterization of water-soluble, heteronuclear ruthenium(III)/ferrocene complexes and their interactions with biomolecules, *J. Inorg. Biochem.*, 2015, **145**, 41-50.
- [28] X. Liu, J. Liang, J. You, L. Ying, Y. Xiao, S. Wang and X. Li, Synthesis and characterization of triphenylamine modified azobenzene dyes-science direct, *Dyes Pigm.*, 2016, **131**, 41-48.
- [29] Y. Liu, M. Nishiura, Y. Wang and Z. Hou, ChemInform abstract: Synthesis and characterization of benzo[c]thiophene analogues tethered with dibenzo-heterocycles as potential OLEDs, *J. Am. Chem. Soc.*, 2006, **128**, 5592-5593.
- [30] Z. Liu, I. Romero-Caneln, B. Qamar, J. M. Hearn, A. Habtemariam, N. P. E. Barry, A. M. Pizarro, G. J. Clarkson and P. J. Sadler, Designing new iridium(III) arene complexes of naphthoquinone derivatives as anticancer agents: a structure–activity relationship study, *Angew. Chem., Int. Ed.*, 2014, **53**, 3941-3946.
- [31] S. Daum, M. S. V. Reshetnikov, M. Sisa, T. Dumych, M. D. Lootsik, R. Bilyy, E. Bila, C. Janko, C. Alexiou, M. Herrmann, L. Sellner and A. Mokhir, Lysosome-targeting amplifiers of reactive oxygen species as anticancer prodrugs, *Angew. Chem., Int. Ed.*, 2017, **56**, 15545-15549.
- [32] C. C. Konkankit, S. C. Marker, K. M. Knopf and J. J. Wilson, In vivo anticancer activity of a rhenium(I) tricarbonyl complex, *Dalton Trans.*, 2018, **47**, 9934-9974.
- [33] L. He, Y. Li, C. Tan, R. Ye, M. Chen, J. Cao, L. Ji and Z. Mao, Cyclometalated iridium(III) complexes as lysosome-targeted photodynamic anticancer and real-time tracking agents, *Chem. Sci.*, 2015, **6**, 5409-5418.

- [34] C. Qian, J. Wang, C. Song, L. Wang, L. Ji and H. Chao, The induction of mitochondria-mediated apoptosis in cancer cells by ruthenium(II) asymmetric complexes, *Metallomics*, 2013, **5**, 844-854. View Article Online
DOI: 10.1039/D0DT02408B
- [35] C. Jin, J. Liu, Y. Chen, G. Li, R. Guan, P. Zhang, L. Ji and H. Chao, Fluorinated cyclometalated iridium(III) complexes as mitochondria-targeted theranostic anticancer agents, *Dalton Trans.*, 2015, **44**, 7538-7547.
- [36] V. Novohradsky, L. Zerzankova, J. Stepankova, A. Kisova, H. Kostrhunova, Z. Liu, P. J. Sadler, J. Kasparkova and V. Brabec, Mitochondria-targeted spin-labelled luminescent iridium anticancer complexes, *Metallomics*, 2014, **6**, 1491-1501.
- [37] L. Wang, M. Li, P. Cao, C. Zhang, F. Huang, F. Xu, B. Liu and M. Zhang, Astin B, a cyclic pentapeptide from *Aster tataricus*, induces apoptosis and autophagy in human hepatic L-02 cells, *Chem.-Biol. Interact.*, 2014, **223**, 1-9.
- [38] C. Ledderose, Y. Bao, M. Lidicky, J. Zipperle, L. L. Li, K. Strasser, N. I. Shapiro and W. G. Junger, Mitochondria are gate-keepers of T cell function by producing the ATP that drives purinergic signaling, *J. Biol. Chem.*, 2014, **289**, 25936-25945.
- [39] T. Chen, Y. Liu, W. Zheng, J. Liu and Y. Wong, Ruthenium polypyridyl complexes that induce mitochondria-mediated apoptosis in cancer cells, *Inorg. Chem.*, 2010, **49**, 6366-6368.
- [40] H. Antonicka, K. Choquet, Z. Y. Lin, A. C. Gingras, C. L. Kleinman and E. A. Shoubridge, A pseudouridine synthase module is essential for mitochondrial protein synthesis and cell viability, *Embo. Rep.*, 2017, **18**, 28-38.
- [41] A. J. Bruce-Keller, J. G. Begley, W. Fu, D. A. Butterfield, D. E. Bredesen, J. B. Hutchins, K. Hensley and M. P. Mattson, Bcl-2 protects isolated plasma and mitochondrial membranes against lipid peroxidation induced by hydrogen peroxide and amyloid β -peptide, *J. Neurochem.*, 1998, **70**, 31-39.
- [42] Y. Zhang, M. Luo, Y. Zu, Y. Fu, C. Gu, W. Wang, L. Yao and T. Efferth, Dryofragin, a phloroglucinol derivative, induces apoptosis in human breast cancer MCF-7 cells through ROS-mediated mitochondrial pathway, *Chem. Biol. Interact.*, 2012, **199**, 129-136.
- [43] A. J. Millett, A. Habtemariam, I. Romero-Canelon, G. J. Clarkson and P. J. Sadler, Contrasting anticancer activity of half-sandwich iridium(III) complexes bearing functionally diverse 2-phenylpyridine ligands, *Organometallics*, 2015, **34**, 2683-2694.
- [44] Z. Liu, R. J. Deeth, J. S. Butler, A. Habtemariam, M. E. Newton and P. J. Sadler, Reduction of quinones by NADH catalyzed by organoiridium complexes, *Angew. Chem., Int. Ed.*, 2013, **52**, 4194-4197.
- [45] Y. Wang, X. Wang, J. Wang, Y. Zhao, W. He and Z. Guo, Noncovalent interactions between a trinuclear monofunctional platinum complex and human serum albumin, *Inorg. Chem.*, 2011, **50**, 12661-12668.
- [46] X. Wei, Y. Yang, J. Ge, X. Lin, D. Liu, S. Wang, J. Zhang, J. Zhou and S. Li, Synthesis, characterization, DNA/BSA interactions and *in vitro* cytotoxicity study of palladium(II) complexes of hispolon derivatives, *J. Inorg. Biochem.*, 2020, **202**, 110857.
- [47] M. E. Pacheco, L. Bruzzone, Synchronous fluorescence spectrometry: Conformational investigation or inner filter effect? *J. Lumin.*, 2013, **137**, 138-142.
- [48] X. He, M. Tian, X. Liu, Y. Tang, C. Shao, P. Gong, J. Liu, S. Zhang, L. Guo and Z. Liu, Triphenylamine-appended half-sandwich iridium^{III} complexes and their biological applications, *Chem. Asian J.*, 2018, **13**, 1500-1509.

- [49] Y. Zhang, B. Zhou, Y. Liu, C. Zhou, X. Ding and Y. Liu, Fluorescence study on the interaction of bovine serum albumin with p-aminoazobenzene, *J. Fluoresc.*, 2008, **18**, 109-118. View Article Online
DOI: 10.1039/D0DT02408B
- [50] M. Carreira, R. Calvo-Sanjuán, M. Sanaú, X. Zhao, R. S. Magliozzo, I. Marzo and M. Contel, Cytotoxic hydrophilic iminophosphorane coordination compounds of d⁸ metals: Studies of their interactions with DNA and HSA, *J. Inorg. Biochem.*, 2012, **116**, 204-214.
- [51] R. Esteghamat-Panah, H. Hadadzadeh, H. Farrokhpour, M. Mortazavi and Z. Amirghofran. A mononuclear Ru(II) complex with meloxicam: DNA- and BSA-binding, molecular modeling and anticancer activity against human carcinoma cell lines, *Inorganica Chimica Acta*, 2017, **454**, 184-196.
- [52] S. Chen, X. Liu, X. Ge, Q. Wang, Y. Xie, Y. Hao, Y. Zhang, L. Zhang, W. Shang and Z. Liu, Lysosome-targeted iridium(III) compounds with pyridine-triphenylamine Schiff base ligands: syntheses, antitumor applications and mechanisms, *Inorg. Chem. Front.*, 2020, **7**, 91–100.

Graphical Abstract

View Article Online
DOI: 10.1039/D0DT02408B

Configuration-modified Fe(II)-Ir(III) heteronuclear metal complexes show potential anticancer activity, especially for *cis*-configurational one.